$SrTiO_3(001)$-$(\sqrt{5}\times\sqrt{5})$-*R*26.6° reconstruction: A surface resulting from phase separation in a reducing environment

David T. Newell,[1] Alastair Harrison,[2] Fabien Silly,[1] and Martin R. Castell[1]
[1]*Department of Materials, University of Oxford, Parks Road, Oxford OX1 3PH, United Kingdom*
[2]*Department of Engineering Science, University of Oxford, Parks Road, Oxford OX1 3PJ, United Kingdom*
(Received 10 October 2006; published 18 May 2007)

Scanning tunneling microscopy (STM) was used to produce atomic resolution images of the Nb-doped $SrTiO_3(001)$-$(\sqrt{5}\times\sqrt{5})$-*R*26.6° reconstruction and its precursor surfaces. Low-energy electron diffraction was used to identify the surface structure in combination with the STM imaging. The $(\sqrt{5}\times\sqrt{5})$-*R*26.6° reconstruction was observed growing as an adlayer on top of the underlying terraces. The formation of this structure could routinely be detected by an increase in the crystal's electrical conductivity during ultrahigh vacuum (UHV) annealing at 1300 °C. This rise in conductivity occurs due to significant reduction of the crystal. Scanning electron microscopy (SEM) on these samples showed small islands with a rectangular base separated by flat regions. Auger electron spectroscopy showed titanium enrichment, and strontium and oxygen depletion of the surface region. The islands seen in the SEM images are TiO crystals, as reported by S. B. Lee *et al.* [Ultramicroscopy **104**, 30 (2005)]. The flat regions between the islands are composed of a Sr adlayer on the surface that is consistent with the $(\sqrt{5}\times\sqrt{5})$-*R*26.6° adatom model of Kubo and Nazoye [Phys. Rev. Lett. **86**, 1801 (2001)]. We propose that the TiO islands and the $(\sqrt{5}\times\sqrt{5})$-*R*26.6° Sr adlayer reconstruction form due to phase separation in the surface region of the crystal. This phase separation is driven by oxygen depletion which occurs during high-temperature UHV annealing of the sample.

DOI: 10.1103/PhysRevB.75.205429 PACS number(s): 68.37.Ef, 68.35.Bs, 82.80.Pv

I. INTRODUCTION

Strontium titanate (STO) is a perovskite oxide with dielectric and ferroelectric properties that are of interest for numerous technological applications. It has been successfully used as a lattice matched substrate for the growth of high-T_c superconducting films.[1,2] Its electronic properties have been investigated for use in transistor technology as an alternative high-*k* crystalline dielectric for complementary metal oxide semiconducting devices,[3–5] dynamic random access memory devices,[6] and also for storage capacitor applications. The STO lattice parameter allows it to be used as a buffer layer to enable epitaxial growth of GaAs on silicon.[7] The material is also noted for its photocatalytic[8] and optical properties.[9] Surface terminations of STO have been used as a substrate for the epitaxial growth of metal nanocrystals and thin films,[10–24] and for TiO_x (Refs. 25–27) or SrO (Refs. 28–30) island growth. For many of these applications the surface structure is of key significance, for example, during the growth of the STO buffer layer between Si and GaAs. Additionally, the nature of the surface reconstruction has been shown to be a significant parameter in determining the shape of epitaxial metal nanocrystals.[12] Therefore, a prime driver for technological applications is to develop reliable processing procedures that will allow the production of specific STO surface terminations.

A number of treatment processes are known to affect the reconstructions of the STO(001) surface. These include annealing time and temperature, the reducing or oxidizing extent of the sample's environment, and Ar^+ bombardment of the surface. Reconstructions with a periodicity of (2×1),[31,32] (2×2),[17] and two forms of $c(4\times4)$,[33,34] have been reported by annealing in a reducing UHV environment up to temperatures of 1200 °C. Annealing in an oxidizing environment has been reported to produce a $c(6\times2)$ reconstruction.[35] Ar^+ sputtering followed by annealing results in a $c(4\times2)$ reconstruction[34] and a range of self-assembled nanostructures that pack into (6×2), (9×2), (12×2), (6×8), or (7×4) periodicities.[36,37] Annealing at higher temperatures, above 1200 °C, gives rise to the $(\sqrt{5}\times\sqrt{5})$-*R*26.6° reconstruction. An additional $(\sqrt{13}\times\sqrt{13})$-*R*37.7° (Ref. 38) reconstruction is reported to form with further annealing of the $(\sqrt{5}\times\sqrt{5})$-*R*26.6° surface.

The first images of the $(\sqrt{5}\times\sqrt{5})$-*R*26.6° surface were published by Matsumoto *et al.*[39] For the sake of brevity we will now no longer include the angle when referring to the $(\sqrt{5}\times\sqrt{5})$ reconstruction. The images presented were the first ever atomic resolution images on the STO system, although the authors incorrectly identified the surface as a (2×2) structure. This was later corrected by the authors and the $(\sqrt{5}\times\sqrt{5})$ periodicity was accurately reported.[40] The authors proposed that the bright spots seen in the scanning tunneling microscopy (STM) images arise due to ordering of oxygen vacancies and the associated creation of Ti^{3+} sites. This type of defect had previously been proposed following photoelectron spectroscopy on STO.[41,42] It was supported by modeling performed by Tsukada *et al.*[43,44] and later by Kimura *et al.*[45] Matsumoto *et al.* demonstrated the growth of thin $SrTiO_3$ films by laser molecular beam epitaxy[46] which gave rise to a $(\sqrt{5}\times\sqrt{5})$ structure when heated. Additionally Tanaka *et al.*[47] reported on the interaction of oxygen molecules with the species identified as oxygen vacancies in STM imaging by Matsumoto *et al.* The Ti^{3+}-oxygen vacancy complex interpretation of the $(\sqrt{5}\times\sqrt{5})$ structure prevailed for a number of years until challenged by the work of Kubo and Nazoye who identified discrepancies between STM images and modeling predictions. The authors proposed a Sr adatom model which

was supported by atomic force microscopy and STM imaging as well as *ab initio* calculations.[48] Kubo and Nazoye extended the Sr adatom model to describe many of the other reconstructions observed on the STO(001) surface.[38] The authors reported that a $(\sqrt{5}\times\sqrt{5})$ surface evolved from a $c(4\times4)$ surface when samples were annealed at 1200 °C for several seconds and that a $(\sqrt{13}\times\sqrt{13})$-*R*37.7° reconstruction evolved from a $(\sqrt{5}\times\sqrt{5})$ surface when the sample was annealed further at 1250 °C for several seconds. The short annealing times and small increase in annealing temperature from 1200 to 1250 °C was suggested by the authors to indicate that the transition is a structural transition rather than a change in the surface composition. Liborio *et al.*[49] performed first-principles total energy calculations for a number of the Sr adatom structures proposed by Kubo and Nazoye. The authors concluded that only structures with a Sr adatom coverage between a narrow range were stable and only when the substrate was in equilibrium, or very close to equilibrium with SrO. This range of stability included the $(\sqrt{5}\times\sqrt{5})$ and the (2×2) reconstructions. Reconstructions with lower Sr coverage, such as the $c(4\times4)$ and the $(\sqrt{13}\times\sqrt{13})$-*R*37.7° were only stable if the system was far from equilibrium, in a transient state where Sr is being lost into the vacuum. These Sr-terminated structures are at odds with the majority of reports on the STO surface, as all other reconstructions with the exception of the $(\sqrt{5}\times\sqrt{5})$ have been characterized as Ti terminations.

It is important to distinguish between a surface being Sr terminated and Sr rich. Although the structure proposed by Kubo and Nazoye is terminated by Sr adatoms the spacing of these atoms means that the underlying TiO_2 (1×1) termination presents a greater number of Ti atoms to the vacuum than the number of Sr atoms in the overlayer. This means that the Auger electron spectroscopy (AES) signal generated from the top monolayers of the surface will still be Ti rich.

TiO_x and SrO islands have been reported on the STO surface. Silly and Castell[27] show the formation of TiO_2 anatase on STO(001) using STM imaging. These anatase islands form following annealing of a nanostructured STO sample in UHV for 1 h at 1200 °C. Lee *et al.*[26] show transmission electron microscopy images of TiO crystals formed on the STO(001) surface. These TiO crystals appear following annealing above 970 °C in a high vacuum (10^{-6} Pa), for times greater than 1 h. It is shown that a carbon layer on the surface assisted in the early stages of the formation of these islands but was not essential for island growth. Gunhold *et al.*[25] show that Ti_2O_3 islands form on STO(001) following the annealing of 0.1 at. % La-doped samples under reducing conditions ($P_{O2}\leq10^{-6}$ Pa), between 1000 and 1300 °C for 2 h. In contrast to this Szot and Speier[28] report on the formation of SrO crystals on the STO(001) surface and present images gained using atomic force microscopy. The islands are chemically characterized using secondary ion mass spectrometry and x-ray photoelectron spectroscopy. The islands were shown to form following annealing in oxygen at temperatures of 1100 °C for 120 h. Rahmati *et al.*[29] report the evolution of SrO island formation by annealing reduced polycrystalline STO samples in an oxidizing environment at 1200 °C for 30 h. The formation of SrO islands was shown to depend on the orientation of the grain direction with the greatest density of SrO islands on the grains with exposed (111) surfaces. Further work by Gunhold *et al.*[30] shows that the formation of SrO islands only occurs when annealing under oxidizing conditions and are not seen when samples are annealed in UHV. They also show that the appearance of SrO is strongly dependent on the concentration of dopants in the crystal, with greater dopant levels encouraging island growth. SrO was not seen at dopant levels of 0.1 at. % La or lower.

Many papers addressing the nature of the chemistry of islands and reconstructions formed on the STO(001) surface focus on enrichment of a single species, i.e., whether the surface is Sr or Ti rich. Instead we propose that the $(\sqrt{5}\times\sqrt{5})$ reconstruction on STO(001) occurs due to phase separation driven by reduction of the surface region. If the separate species produced from this phase separation are unable to sublimate during annealing, then they must be accommodated within the crystal. This material may exist within the sample as point defects, extended phases or may segregate to the surface to create islands or overlayers. SrO-rich Ruddlesden-Popper phases[50,51] are known to form in the bulk of STO. Additionally, SrO and TiO_x islands are reported to form on the surface. However, the authors could find no reports in the current literature regarding stable Ti-rich phases formed within bulk STO. With the exception of the Kubo and Nazoye $(\sqrt{5}\times\sqrt{5})$ reconstruction, the prevailing models for all of the other reconstructions on STO(001) have Ti-terminated surfaces. Whereas the $(\sqrt{5}\times\sqrt{5})$ Sr adatom model may initially look at odds with the majority of the STO(001) reconstructions, in this paper we show experimental results which demonstrate a phase separation of STO into Sr and TiO during UHV annealing at high temperatures. The severe reducing conditions give rise to coexisting $(\sqrt{5}\times\sqrt{5})$ reconstructed strontium-terminated surfaces and TiO islands.

II. EXPERIMENTAL

Single-crystal STO samples were provided by PI-KEM Ltd., UK, with epipolished (001) surfaces and 0.5 wt % Nb doping to achieve *n*-type behavior by substitution of Nb^{5+} on a Ti^{4+} site. Doping is required so that the STO crystals are electrically conducting and hence can be used for STM experiments. These samples were introduced into the UHV system of the STM (JEOL JSTM-4500S) operating at a base pressure of 10^{-8} Pa. The samples were annealed at temperatures up to 1500 °C by resistive direct current heating through the sample. A Thurlby Thandar QL355P power supply was programmed to provide a constant power heating condition. The sample temperatures were measured through a viewport using a Leeds and Northrup disappearing filament optical pyrometer. W tips used for STM imaging were electrochemically etched in a sodium hydroxide solution and then sharpened by milling in a Philips FEI 200 focused ion beam microscope. These tips were used to provide room temperature constant current STM images. On a chamber connected to the STM UHV system there are facilities for UHV scanning electron microscopy (SEM) and AES. The SEM is a JEOL TM Z9043T operating with an accelerating

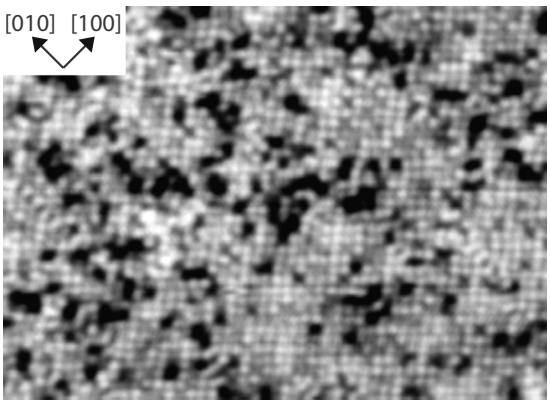

FIG. 1. STM image showing the $c(4\times4)$ STO(001) surface produced by annealing polished samples in UHV (64×46 nm^2, $V_s=+2$ V, $I_t=0.2$ nA).

voltage of 12 kV. AES was performed using the focussed electron beam of the SEM to generate Auger electrons that were energy analyzed using a SPECS PHOIBOS 100. The signal to noise ratio of this system is sufficiently high so that no lock-in amplification techniques are required and the spectra can be read as the primary signal without the need for differentiation. The high spatial resolution and good quality of the AES signal allows quantitative analysis of the data which can be related to the areas scanned in the STM. *Ex situ* SEM imaging was performed with a Hitachi S4500II at 1 keV incident beam energy. Low-energy electron diffraction (LEED) patterns were produced using a 4 mesh VG Microtech rear view system and captured with a Cannon SLR digital camera.

III. RESULTS

STO(001) surfaces were prepared by annealing at 1000 °C in UHV for 1 h to form a flat ordered $c(4\times4)$ reconstruction as shown in the STM image in Fig. 1. The evolution of this reconstruction has been described in detail in one of our previous publications.[33] These samples were then annealed in UHV at temperatures above 1350 °C using a constant power heating condition set between 10 and 12 W. An increasing sample conductivity with time was observed which indicates oxygen depletion in the crystal. A graph showing increasing conductivity over time is shown in Fig. 2. A critical point is seen after approximately 80 min at which a significant increase in sample conductivity occurs. Over a number of such experiments a $(\sqrt{5}\times\sqrt{5})$ LEED pattern was observed following this event, whilst a $(\sqrt{5}\times\sqrt{5})$ LEED pattern was never seen prior to the critical increase in conductivity. Although the same LEED patterns could be produced by annealing an as-polished sample under similar conditions, a $c(4\times4)$ reconstructed sample was used as a starting point as it is a clean flat surface that is easily reproduced. By starting with such a sample, we know that any subsequent reconstruction of the surface is not due to the effects of contamination or polishing damage.

On detection of a rapid increase in conductivity the samples were cooled and imaged with the STM at room

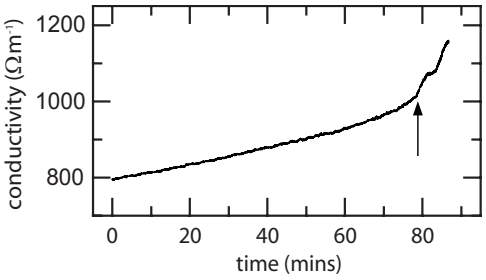

FIG. 2. Plot showing the change in sample conductivity during UHV annealing at 1410 °C. A rapid change in conductivity is seen at approximately 80 min and is associated with the formation of the $(\sqrt{5}\times\sqrt{5})$ reconstruction.

temperature. A typical STM image is seen in Fig. 3(a) showing a surface with large disordered terraces separated by a wavy step edge. On the terraces there are two types of termination, one of which was measured to be 1.51 Å±0.17 Å higher than the other. This is shown in the surface profile in Fig. 3(b), taken horizontally along the direction of the arrow in Fig. 3(a). The profile also shows the step edge corresponding to the STO unit cell height of 3.9 Å. The STM image in Fig. 3(c) shows a region from the higher of the two terminations which contains a degree of order. Groups of periodic spots are seen within the figure, the clearest of which is in the top left corner of the image. A second domain at a different orientation appears below this, which suggests that the structure has at least two possible domain orientations. The average periodicity measured in these domains is 8.77 Å±0.3 Å which corresponds to $\sqrt{5}$ times the STO unit cell. The structure of the lower of the two terminations in Fig. 3(a) could not be determined during this experiment. The LEED pattern of this surface displayed clear (1×1) spots with additional, faint $(\sqrt{5}\times\sqrt{5})$ spots. As the step height between the two terminations shown in Fig. 3 is not an integer value of the STO unit cell size, and because the two terminations appear different to each other in the STM, we conclude that the terminations are chemically or structurally different. The brighter of these two terminations, seen in Fig. 3(a), is a surface adlayer.

Rather than cool immediately upon observing the critical change in conductivity, another set of samples was annealed for a further 5–15 min at 1400–1450 °C. On cooling these samples, the LEED $(\sqrt{5}\times\sqrt{5})$ spots were more intense than those spots generated from the samples cooled immediately on detection of the rise in the sample conductivity. An image of a section of this clearer LEED pattern is shown in Fig. 4(a) next to a simulated image in Fig. 4(b), showing the predicted spot locations for a two domain $(\sqrt{5}\times\sqrt{5})$ surface produced by LEEDPAT software.[52] The pattern in Fig. 4(a) was generated with an incident beam energy of 75 eV and is very crisp suggesting a highly ordered $(\sqrt{5}\times\sqrt{5})$ surface.

STM imaging of samples annealed for fifteen minutes beyond the critical increase in conductivity revealed large flat terraces separated by isolated step edges. A typical STM image of this surface is displayed in Fig. 4(c) and shows a network of white lines covering the surface. This white material is concentrated most strongly at the step edge. Figure 4(d) shows this surface at higher magnification. The white

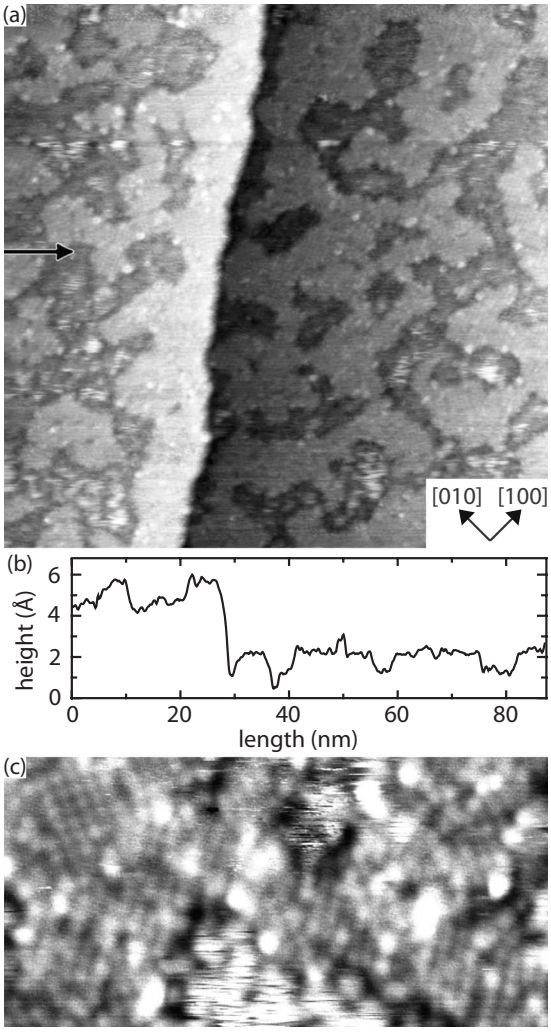

FIG. 3. (a) STM image showing two terminations on the STO(001) surface. A step edge is seen running vertically down the center of the image (99.6×99.6 nm^2, V_s=+1.2 V, I_t=0.1 nA). (b) Profile of the surface displayed in (a), showing a single unit cell step height of approximately 4 Å, and a typical height of approximately 0.15 nm between the two terminations on the terraces. (c) Higher magnification STM image of the brighter termination shown in (a). The surface shows small regions of order that conform to a ($\sqrt{5}\times\sqrt{5}$) periodicity (35.6×17.6 nm^2, V_s=+0.8 V, I_t=0.05 nA).

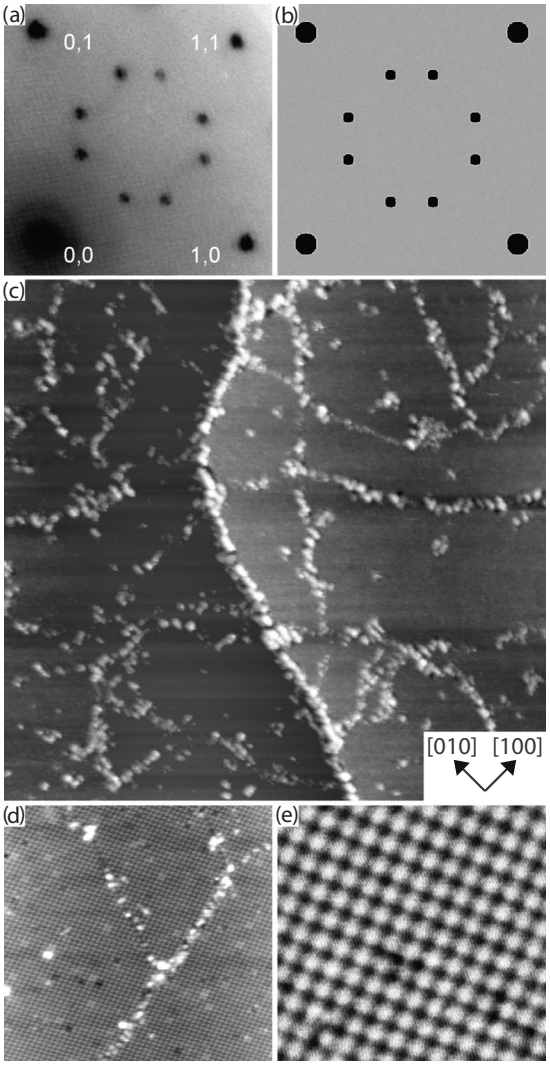

FIG. 4. (a) A unit section of the LEED pattern taken at 75 eV from a ($\sqrt{5}\times\sqrt{5}$) sample with indexed (1×1) spots. (b) LEED pattern simulation of the two domain ($\sqrt{5}\times\sqrt{5}$) reconstruction. (c) STM image showing two terraces on a ($\sqrt{5}\times\sqrt{5}$) surface. A bright network of disordered lines is visible that separates a number of domains (154.7×148.8 nm^2, V_s=+1 V, I_t=0.2 nA). (d) STM image of disordered boundaries which separate three domains of the same orientation (45.4×43.4 nm^2, V_s=+0.9 V, I_t=0.2 nA). (e) Atomic resolution image showing a domain with the ordered ($\sqrt{5}\times\sqrt{5}$) reconstruction (12.4×12.4 nm^2, V_s=−0.8 V, I_t=0.2 nA).

lines are boundaries of disordered material separating ordered ($\sqrt{5}\times\sqrt{5}$) domains. The ordered domain structure is shown further in the STM image in Fig. 4(e). The periodicity of the bright spots has a measured value of 8.68 Å±0.28 Å, which corresponds to the predicted value of the ($\sqrt{5}\times\sqrt{5}$) spacing of 8.732 Å. With typical tunneling currents between 0.05 to 0.3 nA the STM images were insensitive to changes in the sample bias. The ($\sqrt{5}\times\sqrt{5}$) periodicity could be imaged clearly in the whole range of biases between +3.5 to −3.5 V. Throughout this sample bias range, images of the surface remained similar to that seen in the STM image in Fig. 4(e) with round, uniform, bright spots. The ability to image the surface with low positive and negative sample biases indicates that the surface is metallic.

($\sqrt{5}\times\sqrt{5}$) reconstructed samples with a surface structure similar to those shown in Fig. 4 were reheated to temperatures of approximately 1400 °C for periods of 15–20 min. The samples were then cooled and imaged again in the STM. The disordered material at step edges and domain boundaries is much reduced from the images seen previously in Fig. 4 and in some regions the disordered material is entirely absent. This allows an accurate step edge height to be measured. One such step edge is shown in Fig. 5(a) and the profile, shown in Fig. 5(b) is taken horizontally across the image from the point marked by the arrow. This gives a value for the step height as 3.91 Å±0.07 Å which is consistent with a single STO unit cell height. Only step heights corresponding to a single unit cell height are observed on this surface. The absence of disordered material at the

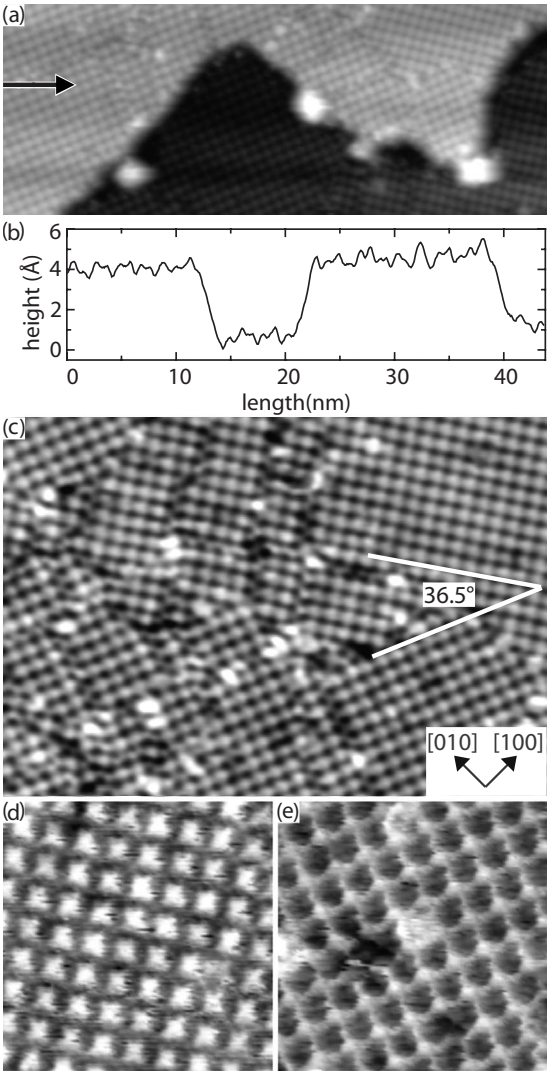

FIG. 5. (a) STM image showing a step edge on the $(\sqrt{5}\times\sqrt{5})$ surface (47.4×18.2 nm^2, $V_s=+1$ V, $I_t=0.5$ nA). (b) Height profile taken from (a) showing a step edge of single unit cell height. The profile is taken horizontally across the surface along the line indicated by the arrow. (c) STM image showing multiple domains of the $(\sqrt{5}\times\sqrt{5})$ surface. Measurement of the angle between two domain orientations is indicated (30.4×21.2 nm^2, $V_s=+1$ V, $I_t=0.5$ nA). (d) STM image showing a $(\sqrt{5}\times\sqrt{5})$ domain with a rotation of −26.6°. The sample is imaged with a positive sample bias and a tunneling current of 1 nA (7.9×7.9 nm^2, $V_s=+0.5$ V, $I_t=1$ nA). (e) STM image of a $(\sqrt{5}\times\sqrt{5})$ domain with a rotation of +26.6°. The sample is imaged with a negative sample bias and a tunneling current of 2 nA (7.9×7.9 nm^2, $V_s=-0.5$ V, $I_t=2$ nA).

boundaries enables clear observation of the angle between the two possible domain orientations. Figure 5(c) shows this angle, which is measured as 36.5° and corresponds to one of the two possible values (53.2° and 36.8°) of the angle between the two $(\sqrt{5}\times\sqrt{5})$ domain orientations.

Although STM images appeared insensitive to changes in the sample bias with tunneling currents below 0.3 nA, images obtained with tunneling currents above 1 nA do show a dependence on the sample bias. High magnification STM images of two separate domain regions imaged at high tunneling currents are shown in Figs. 5(d) and 5(e). Figure 5(d) shows the empty states image, with the surface at a positive sample bias. The bright spots have a squarer shape than the round features seen in Fig. 4(e). Figure 5(e) shows the filled states, with the surface imaged at negative bias values. In this image the periodic spots are now dark with a brighter region surrounding them giving the appearance of a bright grid. Direct comparison between Figs. 5(d) and 5(e) cannot be made as the images obtained at a positive sample bias were obtained from a different region of the sample than the images with a negative bias. This means that the bright features in Fig. 5(d) cannot be related to any of the bright lines or dark spots in Fig. 5(e).

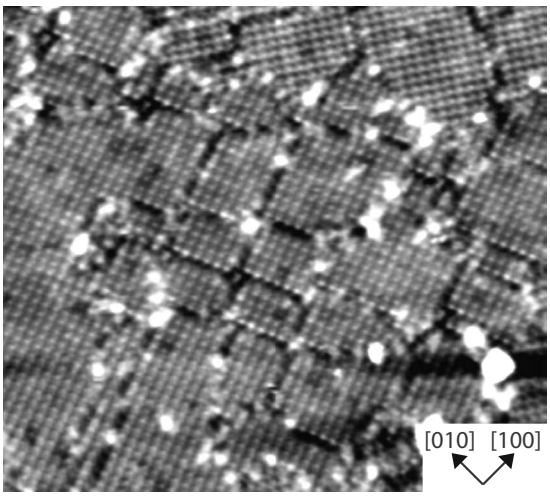

FIG. 6. STM image showing antiphase boundaries separating regions of a single orientation of STO(001)-$(\sqrt{5}\times\sqrt{5})$ (47.7×42.4 nm^2, $V_s=+1$ V, $I_t=0.5$ nA).

Further structural features are seen in the form of antiphase boundaries (APBs), as seen in the STM images in Figs. 5(c) and 6. These APBs are lines separating two regions of an ordered lattice of the same orientation, but the two regions either side of the boundary are shifted with respect to each other. The width of some of these boundaries is less than the $\sqrt{5}$ value, as seen in Fig. 5(c). In Fig. 6 the majority of the boundaries are greater than a $\sqrt{5}$ unit distance.

A STO sample with a $(\sqrt{5}\times\sqrt{5})$ surface structure similar to that seen in Fig. 4 was imaged in the UHV SEM. Imaging of the surface revealed a number of islands of width up to approximately 50 nm. In some regions of the sample the density of these islands is much greater and additional islands are seen that have a longer, rectangular shape. One such region of an area covered by a higher density of islands is shown in the high-resolution SEM image in Fig. 7. This image was obtained by removing the sample from UHV and transferring it to a Hitachi high-resolution SEM operating at 1 keV. Figure 7 shows that the long islands have their edges orientated along the ⟨100⟩ type directions. A number of brighter square shaped features are also seen that have straight sides of approximately 50 nm, orientated along the ⟨110⟩-type directions. We believe the long islands are the same features investigated by Lee *et al.*[26] and identified as TiO islands.

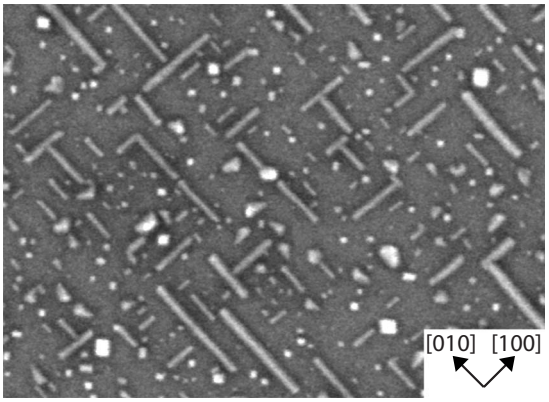

FIG. 7. Secondary electron image of a STO(001)-($\sqrt{5}\times\sqrt{5}$) reconstructed sample. The image shows a number of topographical features on the surface. The largest of these are long islands that are orientated along the ⟨100⟩ directions (1.42×1.03 μm^2, 1 keV).

Auger electron spectra were taken of the $c(4\times4)$, the ($\sqrt{5}\times\sqrt{5}$) surface, and a UHV cleaved sample. A UHV cleaved sample provides a clean surface for AES which has not been modified by annealing in the vacuum. This gives peak heights for Ti, O, and Sr that are as close as possible to representing the composition of the bulk. Figure 8(a) shows the AES spectrum for the UHV cleaved sample. The peaks at 380 and 413 eV arise from Ti (*LMM*), the peaks at 492 and 511 eV are from O (*KLL*), and the Sr (*LMM*) peaks occur at 1644 and 1711 eV. Between the O peaks and the Sr peaks the spectrum has a featureless region with constant gradient. This extends from approximately 550 to 1400 eV and appears to be independent of the nature of the surface. Auger spectra were normalized so that the featureless regions of each spectrum overlapped. This was done by setting the intensity at 1100 eV (a point in the featureless region) to 1000 counts on each spectrum. Following normalization the peak heights of all Auger spectra can be compared quantitatively. The $c(4\times4)$ sample shows Ti enrichment over the UHV cleaved samples, along with oxygen depletion, but a negligible change in the Sr signal. The ($\sqrt{5}\times\sqrt{5}$) sample shows much greater Ti enrichment, more oxygen depletion, and a clear reduction in Sr. Figure 8(b) shows a detailed spectrum between 325 and 575 eV, for the Ti (*LMM*) and the O (*KLL*) peaks on both the cleaved and the ($\sqrt{5}\times\sqrt{5}$) sample. By subtracting the spectrum of the cleaved sample from that of the ($\sqrt{5}\times\sqrt{5}$) surface a difference spectrum is obtained. This difference spectrum is shown in Fig. 8(c) and highlights changes in the composition of the ($\sqrt{5}\times\sqrt{5}$) surface compared to the bulk values. Figure 8(d) shows a detailed spectrum between 1460 and 1760 eV for the Sr (*LMM*) peaks. Figure 8(e) shows the difference spectrum for Sr between the ($\sqrt{5}\times\sqrt{5}$) surface and the UHV cleaved surface.

Figure 9 shows high-resolution spectra of the titanium peak at 413 eV for the $c(4\times4)$ and the ($\sqrt{5}\times\sqrt{5}$) surface. There is a significant difference in the peak shape resulting from the two samples. The peak shape of the $c(4\times4)$ surface, seen in Fig. 9(a), is representative of the peaks also seen on the UHV cleaved surface and all other STO(001) surfaces that we have observed. The $c(4\times4)$ sample has a

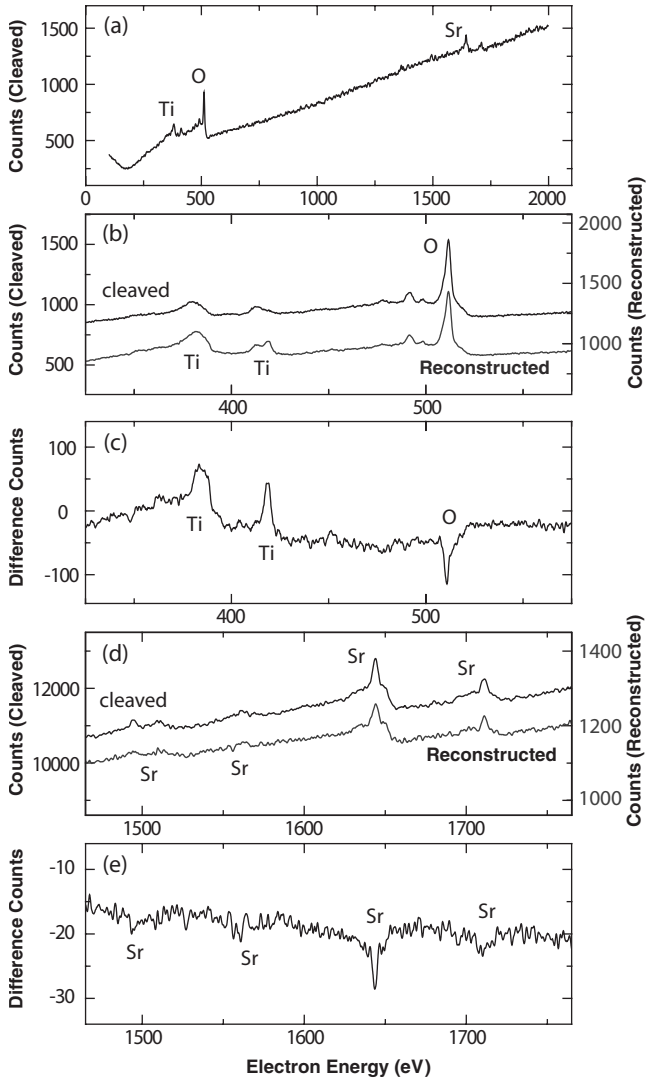

FIG. 8. (a) AES spectrum of a UHV cleaved sample showing the peaks related to Ti (*LMM*) at 380 and 413 eV, O (*KLL*) at 492 and 511 eV, and Sr (*LMM*) at 1644 and 1711 eV. (b) Detailed AES spectra showing the Ti (*LMM*) and O (*KLL*) peaks resulting from spectra generated from a ($\sqrt{5}\times\sqrt{5}$) and a UHV cleaved sample. (c) Difference spectrum showing the subtraction of the UHV cleaved spectrum from the ($\sqrt{5}\times\sqrt{5}$) spectrum shown in (b). This highlights the changes in the surface composition resulting from the formation of a ($\sqrt{5}\times\sqrt{5}$) reconstruction. (d) Detailed AES spectra showing the Sr (LMM) peaks of a ($\sqrt{5}\times\sqrt{5}$) and a UHV cleaved sample. (e) Difference spectrum showing the subtraction of the UHV cleaved spectrum from the ($\sqrt{5}\times\sqrt{5}$) spectrum in (d).

peak at an energy of 413 eV and a shoulder at 419 eV. For the ($\sqrt{5}\times\sqrt{5}$) spectrum in Fig. 9(b) the shoulder seen previously at 419 eV on the $c(4\times4)$ sample now appears as a peak on the ($\sqrt{5}\times\sqrt{5}$) sample, whilst the peak that was seen at 413 eV now appears as a shoulder. A change in the Ti peak shape at 416 eV on a differentiated spectrum was first reported by Lo and Somorjai[53] when investigating the effects of sputtering and annealing on the STO(111) surface. Melnik *et al.*[54] report that the structure of this peak is sensitive to chemical bonding. Our own work investigating the reconstructions on STO(111) (unpublished), suggests that the Ti

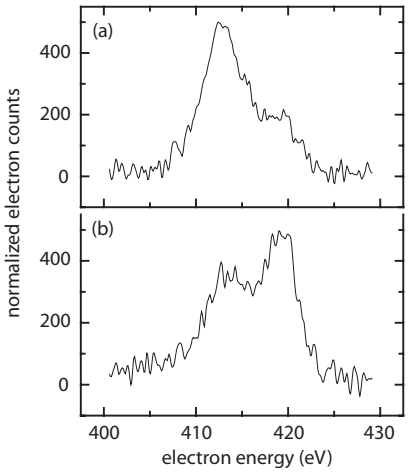

FIG. 9. (a) AES spectra showing the titanium (*LMM*) peak at 413 eV generated from a $c(4\times4)$ surface. (b) AES spectra showing the titanium (*LMM*) peak at 413 eV generated from a $(\sqrt{5}\times\sqrt{5})$ surface.

peak at 413 eV results from Ti^{4+} ions. Whereas the Ti peak at 419 eV is due to Ti^{2+} ions.

The peak heights of Sr, Ti, and O can be compared between the UHV cleaved, $c(4\times4)$, and the $(\sqrt{5}\times\sqrt{5})$ sample using the peaks for Ti at 380 eV, O at 511 eV, and Sr at 1644 eV. The peak heights resulting from the UHV cleaved sample are assumed to represent the stoichiometry of the bulk, as the sample has not been annealed. Comparison of the peak heights generated from the reconstructed surfaces to the peak heights generated from the cleaved sample allows the near surface stoichiometries to be calculated. This gives values for the $c(4\times4)$ surface as $Sr_{0.96}Ti_{1.24}O_{2.85}$ and for the $(\sqrt{5}\times\sqrt{5})$ surface as $Sr_{0.74}Ti_{1.72}O_{2.55}$.

IV. DISCUSSION

The experimental data show that after annealing a STO(001) sample with an ordered $c(4\times4)$ reconstruction above 1350 °C a critical point occurs when the ordered state seen in Fig. 1 is lost and a more disordered two termination surface forms, as shown in Fig. 3. The upper termination is an adlayer with $(\sqrt{5}\times\sqrt{5})$ periodicity. Samples annealed for longer periods do not have surfaces with two terminations but instead are entirely covered by $(\sqrt{5}\times\sqrt{5})$ domains, as seen in Fig. 4. The increase in the sample conductivity at the critical transformation point shown in Fig. 2 suggests that the surface reconstructs due to significant reduction of the crystal. From the magnitude of the increase in the sample conductivity, we infer that the region of the crystal that is significantly oxygen depleted is greater than the top few surface monolayers and extends into the bulk region.

When all of the flat surfaces visible in the STM are reconstructed with a $(\sqrt{5}\times\sqrt{5})$ periodicity similar to the STM image seen in Fig. 4, then SEM imaging of the sample shows islands on the surface. Over many experiments, a large number of island structures were seen on all samples that were covered by a $(\sqrt{5}\times\sqrt{5})$ reconstruction. Lee *et al.*[26] report similar islands on the STO(001) surface following annealing under reducing conditions. Using transmission electron microscopy the authors showed these islands to be TiO. We believe that the islands shown in Fig. 7 are also TiO as they too form under similar highly reducing annealing conditions. This conclusion is supported by the AES spectrum in Fig. 8(c) which is taken from a region of a $(\sqrt{5}\times\sqrt{5})$ sample which has a high density of islands covering the surface. The large coverage of islands means that the spectrum describes the islands rather than the flat $(\sqrt{5}\times\sqrt{5})$ covered regions. The spectrum shows that the islands are Ti rich and oxygen depleted. Additionally, Fig. 9 shows that the Ti (*LMM*) peak shape at 413 and 419 eV is different on the $(\sqrt{5}\times\sqrt{5})$ surface compared to the $c(4\times4)$ surface. This change in peak shape indicates that much of the Ti present on a $(\sqrt{5}\times\sqrt{5})$-terminated sample exists as Ti^{2+} ions, rather than Ti^{4+} ions which are typically found with other STO(001) reconstructions. The fact that TiO islands are always found on $(\sqrt{5}\times\sqrt{5})$ reconstructed samples suggests that these two structures are linked.

To understand the link between the TiO islands and the $(\sqrt{5}\times\sqrt{5})$ reconstruction, it is helpful to consider what happens when $SrTiO_3$ is reduced. When a sample is annealed in UHV, oxygen sublimates from the surface region generating oxygen vacancies. When the number of oxygen vacancies is low, they can be accommodated in the bulk as point defects. However, if a sample is annealed at sufficiently high temperatures, a point may be reached when the rate of oxygen lost from the surface region into the vacuum is greater than the rate at which oxygen can be replenished from the bulk. This results in a surface region that is heavily reduced and not in equilibrium with the bulk. With continued oxygen loss, a critical point will be reached when the perovskite structure can no longer accomodate all the oxygen vacancies and phase separation will occur. If the situation is considered where the STO surface region is reduced to SrTiO stoichiometry then the surface region may separate into Sr and TiO. TiO is found in the form of islands on samples that are covered with a $(\sqrt{5}\times\sqrt{5})$ reconstruction. However, if this arises from a process of phase separation then we must consider what happens to the Sr atoms. At the anneal temperatures involved we would expect some Sr sublimation, but the remainder will be left on the surface.

Kubo and Nazoye[48] propose that the $(\sqrt{5}\times\sqrt{5})$ reconstruction is a Sr adlayer on a TiO_2-terminated STO surface. This surface is proposed to be conducting due to Sr adatoms donating their outermost 5*s* electron to partially fill the conduction band of the underlying TiO_2 termination. This model fits with the flat reconstructed regions shown in this paper, as we show a termination with $(\sqrt{5}\times\sqrt{5})$ periodicity growing as an adlayer between the TiO islands. This adlayer is metallic as images such as those seen in Figs. 4 and 5 could be produced using both very low positive and negative sample biases. A Sr adlayer model of the $(\sqrt{5}\times\sqrt{5})$ reconstruction also fits with the concept of phase separation, as it accounts for the Sr trapped at the surface when TiO islands form.

The implications of phase separation of the STO surface region into TiO islands and a $(\sqrt{5}\times\sqrt{5})$ Sr adatom reconstructed overlayer are that equilibrium models of surface

structure only containing one phase are no longer appropriate. Instead, the whole system needs to be considered, taking into account the coexistence of the $(\sqrt{5}\times\sqrt{5})$ reconstruction and the TiO islands.

Despite the AES results showing that a $(\sqrt{5}\times\sqrt{5})$ covered sample has a titanium-rich surface, this surface may still be Sr terminated. This is because the spacing of Sr adatoms on the surface means that more Ti atoms from the underlying TiO_2 (1×1) reconstructed surface are presented to the vacuum than Sr atoms in the adlayer. This means that the AES signal detected from the reconstructed region will be Ti rich. Additionally the TiO islands are likely to contribute a strong signal to the spectrum resulting in a large Ti signal being detected from the sample as a whole. The Kubo and Nazoye Sr adatom model may appear unusual when all other STO(001) reconstructions are predominantly accepted as Ti terminated. However, it may still be the most appropriate description of the $(\sqrt{5}\times\sqrt{5})$ reconstruction.

V. CONCLUSION

Annealing a STO(001) sample in UHV gives rise to phase separation of the surface region into a $(\sqrt{5}\times\sqrt{5})$ reconstructed Sr adlayer and TiO islands. This phase separation is driven by significant reduction of the crystal. The $(\sqrt{5}\times\sqrt{5})$ reconstruction is best described by the Kubo and Nazoye Sr adatom model but it may only be stable as a component of a phase separated system and may not exist without the coexistence of TiO islands. The process of phase separation on the STO(001) surface may have implications for other highly reduced complex oxides.

ACKNOWLEDGMENTS

The authors would like to thank Oxford Applied Research and the EPSRC for funding and Chris Spencer (JEOL, UK) for valuable technical support.

[1] R. Sum, H. P. Lang, and H.-J. Güntherodt, Physica C **242**, 174 (1995).
[2] K. Endo, P. Badica, and J. Itoh, Physica C **386**, 292 (2003).
[3] J. M. G. Vilar, G. Gomila, and J. M. Rubi, Phys. Rev. Lett. **81**, 14 (1998).
[4] R. A. McKee, F. J. Walker, and M. F. Chisholm, Science **293**, 468 (2001).
[5] X. Zhang, A. A. Demkov, H. Li, X. Hu, Y. Wei, and J. Kulik, Phys. Rev. B **68**, 125323 (2003).
[6] J. F. Scott, Annu. Rev. Mater. Sci. **28**, 79 (1998).
[7] K. Eisenbeiser, R. Emrick, R. Droopad, Z. Yu, J. Finder, S. Rockwell, J. Holmes, C. Overgaard, and W. Ooms, IEEE Electron Device Lett. **23**, 300 (2002).
[8] J. G. Mavroides, J. A. Kafalas, and D. F. Kolisar, Appl. Phys. Lett. **28**, 241 (1976).
[9] D. Kan, T. Terashima, R. Kanda, A. Masuno, K. Tanaka, S. Chu, H. Kan, A. Ishizumi, Y. Kanemitsu, Y. Shimakawa, and M. Takano, Nat. Mater. **4**, 816 (2005).
[10] F. Silly and M. R. Castell, Phys. Rev. Lett. **96**, 086104 (2006).
[11] K. Sun, S. Zhu, R. Fromknecht, G. Linker, and L. M. Wang, Mater. Lett. **58**, 547 (2004).
[12] F. Silly and M. R. Castell, Phys. Rev. Lett. **94**, 046103 (2005).
[13] T. Wagner, G. Richter, and M. Rühle, J. Appl. Phys. **89**, 2606 (2001).
[14] G. Richter and T. Wagner, J. Appl. Phys. **98**, 094908 (2005).
[15] F. Silly and M. R. Castell, J. Phys. Chem. B **109**, 12316 (2005).
[16] X. Chen, T. Garrent, S. W. Liu, Y. Lin, Q. Y. Zhang, C. Dong, and C. L. Chen, Surf. Sci. **542**, L655 (2003).
[17] F. Silly and M. R. Castell, Appl. Phys. Lett. **87**, 053106 (2005).
[18] T. Conard, A.-C. Rousseau, L. M. Yu, J. Ghijsen, R. Sporken, R. Caudano, and R. L. Johnson, Surf. Sci. **359**, 82 (1996).
[19] D. Vlachos, M. Kamaratos, S. D. Foulias, C. Argirousis, and G. Borchardt, Surf. Sci. **550**, 213 (2004).
[20] F. Silly and M. R. Castell, Appl. Phys. Lett. **87**, 063106 (2005).
[21] E. Tchernychova, C. Scheu, T. Wagner, Q. Fu, and M. Rühle, Surf. Sci. **542**, 33 (2003).
[22] B. Koslowski, R. Notz, and P. Ziemann, Surf. Sci. **496**, 153 (2002).
[23] Q. Fu and T. Wagner, Surf. Sci. **505**, 39 (2002).
[24] F. Silly and M. R. Castell, Appl. Phys. Lett. **87**, 213107 (2005).
[25] A. Gunhold, L. Beuermann, M. Frerichs, V. Kempter, K. Gömann b, G. Borchardt, and W. Maus-Friedrichs, Surf. Sci. **523**, 80 (2003).
[26] S. B. Lee, F. Phillipp, W. Sigle, and M. Rühle, Ultramicroscopy **104**, 30 (2005).
[27] F. Silly and M. R. Castell, Appl. Phys. Lett. **85**, 3223 (2004).
[28] K. Szot, W. Speier, U. Breuer, R. Meyer, J. Szade, and R. Waser, Surf. Sci. **460**, 112 (2000).
[29] B. Rahmati, J. Fleig, W. Sigle, E. Bischoff, J. Maier, and M. Rühle, Surf. Sci. **595**, 115 (2005).
[30] A. Gunhold, K. Gorman, L. Beuermann, M. Frerichs, G. Borchardt, V. Kempter, and W. Maus-Friedrichs, Surf. Sci. **507-510**, 447 (2002).
[31] Q. D. Jiang and J. Zegenhagen, Surf. Sci. **338**, L882 (1995).
[32] N. Erdman, K. R. Poeppelmeier, M. Asta, O. Warschkow, D. E. Ellis, and L. D. Marks, Nature (London) **419**, 55 (2002).
[33] F. Silly, D. T. Newell, and M. R. Castell, Surf. Sci. **600**, L219 (2006).
[34] M. R. Castell, Surf. Sci. **505**, 1 (2002).
[35] Q. D. Jiang and J. Zegenhagen, Surf. Sci. **425**, 343 (1999).
[36] M. R. Castell, Surf. Sci. **516**, 33 (2002).
[37] D. S. Deak, F. Silly, D. T. Newell, and M. R. Castell, J. Phys. Chem. B **110**, 9246 (2006).
[38] T. Kubo and H. Nazoye, Surf. Sci. **542**, 177 (2003).
[39] T. Matsumoto, H. Tanaka, T. Kawai, and S. Kawai, Surf. Sci. **278**, 153 (1992).
[40] H. Tanaka, T. Matsumoto, T. Kawai, and S. Kawai, Jpn. J. Appl. Phys., Part 1 **32**, 1405 (1993).
[41] V. E. Henrich, G. Dresselhaus, and H. J. Zeiger, Phys. Rev. B **17**, 4908 (1978).
[42] B. Cord and R. Courths, Surf. Sci. **162**, 34 (1985).
[43] M. Tsukada, A. Adachi, and C. Satoko, Prog. Surf. Sci. **14**, 113 (1983).
[44] M. Tsukada, C. Satoko, and H. Adachi, J. Phys. Soc. Jpn. **48**, 200

(1980).
[45] S. Kimura, J. Yamauchi, and M. Tsukada, Phys. Rev. B **51**, 11049 (1995).
[46] T. Matsumoto, H. Tanaka, K. Kouguchi, T. Kawai, S. Kawai, and S. Watanabe, Surf. Sci. **312**, 21 (1994).
[47] H. Tanaka, T. Matsumoto, T. Kawai, and S. Kawai, Surf. Sci. **318**, 29 (1994).
[48] T. Kubo and H. Nozoye, Phys. Rev. Lett. **86**, 1801 (2001).
[49] L. M. Liborio, C. G. Sánchez, A. T. Paxton, and M. W. Finnis, J. Phys.: Condens. Matter **17**, L223 (2005).
[50] S. N. Ruddlesden and P. Popper, Acta Crystallogr. **10**, 538 (1957).
[51] S. N. Ruddlesden and P. Popper, Acta Crystallogr. **11**, 54 (1958).
[52] K. Herman and M. A. Van Hove, *LEED pattern simulator*, Version 2.0, 2002.
[53] W. J. Lo and G. A. Somorjai, Phys. Rev. B **17**, 4942 (1978).
[54] V. Melnik, V. Popov, D. Kruger, and O. Oberemok, Semicond. Phys., Quantum Electron. Optoelectron. **2**, 81 (1999).